Earthquakes and Structures, *Vol. 8, No. 1 (2015) 185-204*
DOI: http://dx.doi.org/10.12989/eas.2015.8.1.185

Influence of ground motion selection methods on seismic directionality effects

Cristina Cantagallo*, Guido Camata[a], Enrico Spacone[b]

Engineering and Geology Department, University "G. D'Annunzio" of Chieti-Pescara, Viale Pindaro 42, 65127 Pescara, Italy

(Received June 19, 2014, Revised July 30, 2014, Accepted September 26, 2014)

Abstract. This study investigates the impact of the earthquake incident angle on the structural demand and the influence of ground motion selection and scaling methods on seismic directionality effects. The structural demand produced by Non-Linear Time-History Analyses (NLTHA) varies with the seismic input incidence angle. The seismic directionality effects are evaluated by subjecting four three-dimensional reinforced concrete structures to different scaled and un-scaled records oriented along nine incidence angles, whose values range between 0 and 180 degrees, with an increment of 22.5 degrees. The results show that NLTHAs performed applying the ground motion records along the principal axes underestimate the structural demand prediction, especially when plan-irregular structures are analyzed. The ground motion records generate the highest demand when applied along the lowest strength structural direction and a high energy content of the records increases the structural demand corresponding to this direction. The seismic directionality impact on structural demand is particularly important for irregular buildings subjected to un-scaled accelerograms. However, the orientation effects are much lower if spectrum-compatible combinations of scaled records are used. In both cases, irregular structures should be analyzed first with pushover analyses in order to identify the weaker structural directions and then with NLTHAs for different incidence angles.

Keywords: directionality; ground motion; nonlinear time history analysis; angle of incidence; reinforced concrete structures; ground motion scaling

1. Introduction

In seismic engineering, when Non-Linear Time History Analyses (NLTHA) are used, the seismic load effects are typically computed using two or three orthogonal simultaneously acting seismic horizontal components applied along the principal axes of the analyzed structure. However, in some cases, such as for irregular structures, it may be difficult to define the principal structural axes. Also, during an earthquake, the direction of the dominant excitation component is not necessarily aligned with the principal structural axes and can change during the event. Thus, applying the main seismic component along a direction different from the principal structural axes is of interest as it may lead to higher structural demand. For this reason Eurocode 8 (CEN EN

*Corresponding author, Post doctoral fellow, E-mail: cristina.cantagallo@unich.it
[a]Assistant Professor, E-mail: g.camata@unich.it
[b]Professor, E-mail: espacone@unich.it

http://www.techno-press.org/?journal=sem&subpage=8 ISSN: 1225-4568 (Print), 1598-6217 (Online)

1998-1 2005) states in §4.3.3.1(11)P: "*Whenever a spatial structural model is used, the design seismic action shall be applied along all relevant horizontal directions (with regard to the structural layout of the building) and their orthogonal horizontal axes*. *For buildings with resisting elements in two perpendicular directions these two directions shall be considered as the relevant directions*". Stewart *et al*. (2011) has recently coined the term *azimuth-dependent* structures to identify structures with preferred response directions. These structures are deemed sensitive to the ground motion directionality. Other structures that have same lateral strength and stiffness along all directions and do not have preferred response directions are referred to as *azimuth-independent* structures. Since the relevant directions of an asymmetric complex structure are a priori unknown, several incidence angles should be considered in order to assess the highest structural demand.

Several previous studies on the excitation of multi-component earthquakes and the critical angle of incidence consider a linear structural behavior only. They prevalently use Response Spectrum Analyses RSA (Smeby *et al*. 1985, Wilson *et. al*. 1995, Lopez *et al*. 1997, Menun *et al*.1998) or Linear Time History Analyses LTHA (Lopez *et. al*. 2000, Athanatopoulou 2005). More recently, some authors (Rigato *et al*. 2007, Hosseini *et al*. 2008, Tsourekas *et al*. 2009, Lagaros 2010, Reyes *et al*. 2012, Kalkan *et al*. 2013) have analyzed the effects of ground motion directionality using Non-Linear Time History Analysis NLTHA.

More specifically, Rigato and Medina (2007) studied different symmetrical and asymmetrical structures examining the influence of the ground motion incident angle on several Engineering Demand Parameters (EDPs). The nonlinear structural models are subjected to a set of 39 pairs of accelerograms. Rigato and Medina show that application of bi-directional ground motions along an inelastic building main axes underestimates the inelastic peak deformation demands. The average ratios between the peak deformation responses obtained from all angles of incidence and those obtained by applying ground motions at principal building orientations typically vary between 1.1 and 1.6. However, for individual ground motions these ratios could be as high as 5.0 for the EDPs examined. Hosseini and Salemi (2008) analyze two 5-story steel buildings with NLTHAs, using two simultaneous horizontal components of three earthquakes orientated with different angles of excitation. The results show that column axial forces are strongly influenced by the earthquake incident direction. Furthermore, the maximum axial force in each column is obtained with a specific angle of excitation, which varies for different earthquakes. More recently, Kalkan and Reyes (2013) investigate the influence of ground motion rotational angle analyzing nine symmetric and asymmetric three dimensional structures subjected to a suite of bi-directional near-fault records. The results of NLTHAs show that for a given record and structure, there is no optimum orientation maximizing different EDPs simultaneously. In addition, they found that ground motions oriented along fault-normal/fault-parallel (FN/FP) direction or along maximum direction MD, can lead to an underestimation of the peak demand up to 20%.

The overall objective of this work is to investigate the importance of the ground motion incidence angle by way of NLTHAs of four symmetric and asymmetric structures subjected to two simultaneous horizontal un-correlated components of several ground motion inputs. Each ground motion record is applied with incidence angles varying between 0 and 180 degrees with 22.5 degree increments. Furthermore, this study aims to evaluate how the ground motion selection and modification methods affect the directional effects on seismic demand. For this purpose, the analyzed structures are subjected to two different groups of scaled and un-scaled records and each of them is oriented along the previously described incidence angles.

The scaling criterion used in this study is a mixture between the scaling criterion adopted by the Pacific Earthquake Engineer Research (PEER) center, and part of the Eurocode 8 spectral

compatibility criterion. In the PEER methodology, the spectral ordinate $S_a(T_1)$ is used as an optimal Intensity Measure (IM) and the ground motion records are scaled to the value of the $S_a(T_1)$ corresponding to the specified hazard level. Since the damage of the structure in NLTHA can determinate an elongation of the fundamental periods, $S_a(T_1)$ could be not correlated with the selected EDPs (Cantagallo *et al*. 2012, Faggella *et al*. 2013). Faggella *et al*. 2013 underline the need for a vector-valued IM accounting for spectral ordinates at different periods (or period ranges) of the structure. Other authors (Baker *et al*. 2005) consider a vector-valued IM consisting of two parameters, spectral acceleration at a reference period and epsilon ε, where ε is a measure of the difference between the spectral acceleration of a record and the mean of a ground motion prediction equation at the given period. In order to account for $\varepsilon(T_i)$ in the ground motion selection and modification process, the Conditional Mean Spectrum CMS (Baker 2011) can be used as an alternative to the Uniform Hazard Spectrum UHS. However, in this work the selection and scaling process is based on the UHS as it currently remains the most used tool to carry out the selection and modification of ground motions; the impact of the earthquake incident angle on a ground motion selection based on CMS could be treated in further studies.

2. Reinforced concrete structures and structural models

Four reinforced concrete structures (referred to as Structure 1, Structure 2, Structure 3, Structure 4) are selected according to their structural configuration. They have increasing plan irregularity. The NLTHAs on the structural models shown in Fig. 1 are carried out with the commercial computer software Midas Gen 7.21 using a force-based fiber-section frame model (Spacone *et al*. 1996) with four Gauss-Lobatto integration points for the columns and linear elastic elements for all beams, as the buildings are designed to represent existing structures which predominantly fail because of column failures. Beams of structures 1 to 4 are modeled with a reduced elastic modulus (50%) to consider the section cracked. The beams are modeled elastic because the typical existing RC frame buildings behave as weak columns - strong beams and therefore the plastic hinges are expected to develop in the columns and not in the beams. Rigid diaphragms are used at all floor levels. The concrete is modeled with the Kent and Park (1971) confined constitutive law with f_{ck} = 20 *MPa* and strain at maximum compressive strength ε_{c0} = 0.003. The Menegotto and Pinto (1973) constitutive law is used for the reinforcing steel, with f_{yk} = 215 *MPa* (Structure 3, 4) and 430 *MPa* (Structure 1, 2), E = 200 *GPa* and strain hardening ratio b = 0.02. The f_{yk} values are chosen to represent the material parameters of existing structures built in different historical periods. Gravity loads are applied statically before the ground motion records are dynamically applied to the base of the structures. They are converted to lumped mass data and applied to each floor node. The floor masses used in NLTHA include all dead loads and 30% of live loads according to Eurocode 8.

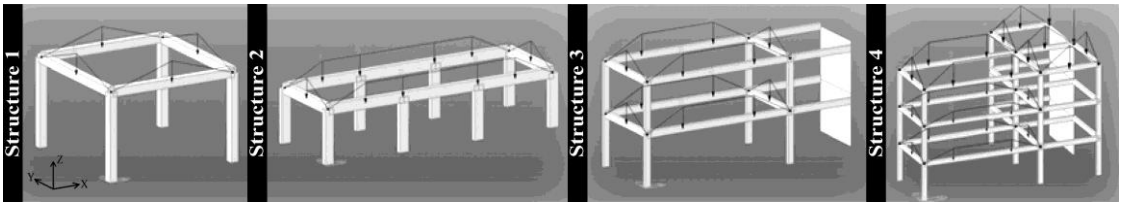

Fig. 1 Structural configuration of Structures 1, 2, 3 and 4 (from left to right)

Structure 1 is a doubly symmetric 1-storey 1-bay frame. The structural configuration is regular, both in terms of mass and stiffness distributions. The beam span is 5 *m* and the column height is 3 *m*: beam and column cross sections are all 30x30 cm. The first three linear periods of the structure are T_1 = 0.17 sec, T_2 =0.17 sec , T_3 = 0.16 sec, and the translational mass participation ratios in the principal structural directions *x, y* and *z* are m_{1x} = 100%, m_{1y} = 0, m_{1z} = 0, m_{2x} = 0, m_{2y} = 100%, m_{2z} = 0, m_{3x} = 0, m_{3y} = 0 and m_{3z} = 100%. The columns are reinforced with four 12 *mm* diameter rebars and their sections are subdivided into 10x10 fibers.

Structure 2 is a 1-storey rectangular multi-bay structure. It can be generally defined as regular, but due to the column geometry, the structure has a longitudinal stiffness that is much higher than the transversal one. The plan dimensions are 15x3 m. The beam and column cross sections are 30x60 cm. The first three linear periods of the structure are T_1 = 0.16 sec, T_2 = 0.11 sec, T_3 = 0.07 sec, and the translational mass participation ratios in the principal structural directions *x*, *y* and *z* are m_{1x} = 0, m_{1y} = 100%, m_{1z} = 0, m_{2x} = 0, m_{2y} = 0, m_{2z} = 100%, m_{3x} = 100%, m_{3y} = 0 and m_{3z} = 0. The columns are reinforced with four 14 mm diameter rebars and their sections are subdivided into 6x12 concrete fibers.

Structure 3 is a 2-storey rectangular multi-bay structure 15×3 m in plan and 6 m high. In addition, a 6 m high, 0.2 m thick reinforced concrete wall is eccentrically placed. The three transverse frames are not equally spaced as the middle frame is placed 2.5 m away from the geometric center. The structure is regular in elevation, but plan-irregular because of the high eccentricity between mass and stiffness centers in the longitudinal direction. The beam and column sections are 20x40 cm. The first three linear periods of the structure are T_1 = 0.52 sec, T_2 = 0.43 sec, T_3 = 0.18 sec and the translational mass participation ratios in the principal structural directions *x*, *y* and *z* are m_{1x} = 0, m_{1y} = 55%, m_{1z} = 35%, m_{2x} = 37%, m_{2y} = 0, m_{2z} = 0, m_{3x} = 0, m_{3y} = 5% and m_{3z} = 6%. The columns are reinforced with four 10 mm diameter rebars and their sections are subdivided in 4x8 concrete fibers. The shear wall is modeled with elastic elements.

Structure 4 is a 3-storey multi-bay structure with a L-shaped plan configuration. A concrete wall (L = 3 m, H = 9 m, t = 0.2 m) is included in the transverse frame and is modeled with elastic elements. The distributions of the structural elements and loads give the structure a significant irregularity both in plan and in elevation. The structure is 15x6 m in plan. Beams, columns and walls are identical to those of Structure 3. The first three linear periods of the structure are T_1 = 0.90 sec, T_2 = 0.76 sec, T_3 = 0.25 sec, corresponding to the mass participation ratios and the translational mass participation ratios in the principal structural directions *x*, *y* and *z* are m_{1x} = 13%, m_{1y} = 37%, m_{1z} = 39%, m_{2x} = 73%, m_{2y} = 7%, m_{2z} = 7%, m_{3x} = 0, m_{3y} = 4% and m_{3z} = 4%.

The selected engineering demand parameter (EDP) used to investigate the effects of the ground motion direction variability on the structural demand is the Maximum Interstory Drift Ratio MIDR. MIDR is computed as the maximum percentage interstory drift DXY over the record duration, that is MIDR = max[DXY(t)]. For each record, the interstory drift ratio at an instant t is computed as

$$\mathrm{DXY}(t) = \sqrt{\mathrm{DX}(t)^2 + \mathrm{DY}(t)^2} \tag{1}$$

where DX(t) and DY(t) are the instantaneous interstory drifts in the X and Y directions, respectively, between the centers of mass of two adjacent floors.

3. Ground motion record selection

The record selection used in this study is based on the Probabilistic Seismic Hazard Analysis (PSHA) derived from an Italian study carried out between 2004 and 2006 by the Italian National Institute of Geophysics and Volcanology (INGV) and the Italian Civil Protection Department (DPC). This work (Meletti *et al*. 2007) provides the seismic hazard analysis and the disaggregation for each point of a regular grid made of approximately 16852 nodes covering the entire Italian territory.

Records are selected using an earthquake scenario with moment magnitude M_w, epicentral distance R and soil site class A. The M_w-R bins providing the larger contribution to the seismic hazard at a specified probability of exceedance (Spallarossa *et al*. 2007) are derived from seismic hazard disaggregation (Bazzurro *et al*. 1999). For the analyses presented in this study, a site located on rock soil in Sulmona (Italy) - 42.084° latitude and 13.962° longitude - is selected. 61 records (each consisting of two orthogonal components), with M_w between 5.5 and 6.5 and R between 15 and 30 km, are selected for a probability of exceedance of 10% in 50 years. Epicentral distances R smaller than 15 km are not considered in order to avoid "near-field" effects. The selected records are taken from two databases: the European Strong-motion Database - ESD (Ambraseys *et al*. 2002) and the ITalian ACcelerometric Archive - ITACA (Luzi *et al*. 2008, Pacor *et al*. 2011). In these databases the ground motion components (two horizontal and one vertical) are given with the orientation in which they are recorded. In general, these components are correlated because the recording instruments are not oriented along the principal directions of the ground motion (Penzien *et al*. 1975). All selected records are then uncorrelated using a coordinate transformation formally identical to that used for stress transformations (López *et al*. 2004).

For each selected record and for any structural period T, a single spectral acceleration $S_a(T)$ is obtained as geometric mean of the two corresponding horizontal spectral components

$$S_a(T) = \sqrt{S_{aX}(T) \cdot S_{aY}(T)} \tag{2}$$

As stated in Beyer and Bommer (2006), the geometric mean is the most widely used definition of the horizontal component of motion. A single spectrum is therefore computed from the spectral values of the X and Y components.

The spectra corresponding to the un-scaled records are then scaled to the spectral acceleration $S_a(T^*)$ corresponding to the "non-linear period" T^*. As shown by a previous study (Cantagallo *et al*. 2012), $S_a(T^*)$ produces the lowest variability in structural demand among the most common input intensity measures. It considers the elongation of the effective structural period during the non-linear analysis and is well correlated with the deformation demand. In order to calculate $S_a(T^*)$ for each record and structure, the "non-linear period" T^* is obtained from non-linear static (pushover) analyses carried out according to Eurocode 8 (CEN EN 1998-1 2005). Following application of the gravity loads to the structures, two distributions of lateral loads are applied to each structure, mainly a "uniform" pattern, based on mass proportional lateral forces, and a "modal" pattern, proportional to the first mode lateral force distribution in the direction under consideration. Capacity curves representing the relation between base shear force and control node displacement are obtained from the Multi Degree of Freedom (MDOF) systems and then transformed into those of equivalent Single Degree of Freedom (SDOF) systems and approximated by a bilinear elasto-perfectly plastic force–displacement curve. T^* is the period corresponding to the initial branch of the bilinear idealized curve and is computed from the Eq. (3)

Table 1 T^* values obtained at the ULS from pushover analyses that apply to each structure a distribution of lateral loads proportional to a "uniform" and "modal" pattern

Distribution	Direction	Structure 1	Structure 2	Structure 3	Structure 4
Uniform Pattern	T^*_x (sec)	**0.35**	0.20	0.77	1.19
Uniform Pattern	T^*_y (sec)	0.35	**0.49**	**0.90**	**1.07**
Modal Pattern	T^*_x (sec)	-	-	0.83	1.31
Modal Pattern	T^*_y (sec)	-	-	1.25	1.61

$$T^* = 2\pi\sqrt{\frac{m^* d_y^*}{F_y^*}} \tag{3}$$

where d_y^* and F_y^* are the yield displacement and the ultimate strength of the bilinear idealized system, respectively, and m^* is the mass of the equivalent SDOF system (CEN EN 1998-1 2005).

The T^* values vary depending on the distribution of lateral loads and the loading direction. In this study only the T^* values corresponding to a "uniform" pattern applied in the direction of the first linear period are used to obtain the scaling factors. Table 1 shows the T^* values computed applying the "uniform" and the "modal" load patterns; the T^* values used in this study are shown in bold.

As for $S_a(T)$, also for the spectral acceleration corresponding to the period T^*, $S_a(T^*)$, a single spectral acceleration is obtained as geometric mean of the two corresponding horizontal components

$$S_a\left(T^*\right) = \sqrt{S_{a\mathrm{X}}\left(T^*\right) \cdot S_{a\mathrm{Y}}\left(T^*\right)} \tag{4}$$

$S_a(T^*)$ value of Eq. (4) is then scaled to the corresponding target spectral acceleration: in this way a single scale factor for both horizontal components of each record. The two so-scaled orthogonal components are then simultaneously applied to the four structures of Fig. 1 along nine different incidence angles.

Since this work focuses on the influence of the ground motion selection and modification methods on the directional effects of the seismic demand, a group of scaled records is obtained from the pre-selected 61 ground motion records. Comb. 1 contains all 61 un-scaled records. Strictly speaking, these 61 records are not spectrum-compatible according to Eurocode 8. Comb. 2 contains 20 scaled and spectrum-compatible records (each with two orthogonal components), selected so that in the $0.2T^*$-$2T^*$ spectrum-compatibility range of Eurocode 8, the mean elastic spectrum calculated from all time histories is within the 90% to 110% window of the uniform hazard spectrum. Eurocode 8 spectrum-compatibility criterion requires that a) the mean of the peak ground accelerations PGAs calculated from the individual time histories should not be smaller than the PGA obtained from the PSHA; b) in the range of periods $0.2T_1$ - $2T_1$ (where T_1 is the fundamental period of the structure), no value of the elastic spectrum calculated from all time histories should be less than 90% of the corresponding value of the elastic response spectrum. In the current study, only condition b) is imposed to the scaled records, adding a 110% upper bound to the existing 90% lower bound.

Table 2 Ground motion records

Database	ID number	Earthquake Name	Station Code	Date	Site Class	Moment Magnitude M_w	Epicentral Distance R (km)
ESD	000055	Friuli	ST20	06/05/1976	A	6.5	23
ESD	000128	Friuli (aftershock)	ST36	15/09/1976	A	6	28
ESD	000212	Montenegro (aftershock)	ST68	15/04/1979	A	5.8	22
ESD	000234	Montenegro (aftershock)	ST68	24/05/1979	A	6.2	30
ESD	000246	Valnerina	ST61	19/09/1979	A	5.8	22
ESD	000359	Umbria	ST136	29/04/1984	A	5.6	17
ESD	000362	Umbria	ST137	29/04/1984	A	5.6	27
ESD	000363	Umbria	ST138	29/04/1984	A	5.6	27
ESD	000368	Lazio Abruzzo	ST143	07/05/1984	A	5.9	22
ESD	000382	Lazio Abruzzo (aftershock)	ST140	11/05/1984	A	5.5	16
ESD	000385	Lazio Abruzzo (aftershock)	ST155	11/05/1984	A	5.5	15
ESD	000410	Golbasi	ST161	05/05/1986	A	6	29
ESD	000597	Umbria Marche	ST222	26/09/1997	A	5.7	24
ESD	000598	Umbria Marche	ST222	26/09/1997	A	6	27
ESD	000626	Umbria Marche (aftershock)	ST222	06/10/1997	A	5.5	29
ESD	000638	Umbria Marche (aftershock)	ST233	14/10/1997	A	5.6	17
ESD	000639	Umbria Marche (aftershock)	ST226	14/10/1997	A	5.6	29
ESD	000641	Umbria Marche (aftershock)	ST84	14/10/1997	A	5.6	26
ESD	000642	Umbria Marche (aftershock)	ST225	14/10/1997	A	5.6	23
ESD	000646	Umbria Marche (aftershock)	ST234	14/10/1997	A	5.6	17
ESD	000647	Umbria Marche (aftershock)	ST222	14/10/1997	A	5.6	27
ESD	000650	Umbria Marche (aftershock)	ST235	14/10/1997	A	5.6	23
ESD	000661	Umbria Marche	ST238	26/09/1997	A	5.7	24
ESD	000665	Umbria Marche	ST238	26/09/1997	A	6	21
ESD	000670	Umbria Marche (aftershock)	ST238	06/10/1997	A	5.5	20
ESD	000763	Umbria Marche	ST266	26/09/1997	A	5.7	23
ESD	000764	Umbria Marche	ST266	26/09/1997	A	6	25
ESD	000949	Sicilia-Orientale	ST291	13/12/1990	A	5.6	29
ESD	000990	Lazio Abruzzo (aftershock)	ST313	11/05/1984	A	5.5	15
ESD	001243	Izmit (aftershock)	ST575	13/09/1999	A	5.8	15
ESD	001891	Kranidia	ST1320	25/10/1984	A	5.5	23
ESD	004557	Bovec	ST750	12/04/1998	A	5.6	25
ESD	005270	Mt. Vatnafjoll	ST2486	25/05/1987	A	6	25
ESD	005272	Mt. Vatnafjoll	ST2487	25/05/1987	A	6	24
ESD	005615	Friuli (aftershock)	ST36	11/09/1976	A	5.5	26
ESD	006115	Kozani	ST1320	13/05/1995	A	6.5	17
ESD	006265	South Iceland	ST2494	17/06/2000	A	6.5	29

Table 2 Continued

Database	ID number	Earthquake Name	Station Code	Date	Site Class	Moment Magnitude M_w	Epicentral Distance R (km)
ESD	006277	South Iceland	ST2558	17/06/2000	A	6.5	15
ESD	006327	South Iceland (aftershock)	ST2552	21/06/2000	A	6.4	24
ESD	006331	South Iceland (aftershock)	ST2486	21/06/2000	A	6.4	22
ESD	006333	South Iceland (aftershock)	ST2487	21/06/2000	A	6.4	28
ESD	006335	South Iceland (aftershock)	ST2557	21/06/2000	A	6.4	15
ESD	006336	South Iceland (aftershock)	ST2563	21/06/2000	A	6.4	24
ESD	006341	South Iceland (aftershock)	ST2497	21/06/2000	A	6.4	20
ESD	006342	South Iceland (aftershock)	ST2556	21/06/2000	A	6.4	20
ESD	007156	Firuzabad	ST3291	20/06/1994	A	5.9	21
ESD	007187	Avej	ST3311	22/06/2002	A	6.5	28
ITACA	IT0083	Friuli earthquake 2nd shock	SMT	11/09/1976	A	5.6	20.2
ITACA	IT0090	Friuli earthquake 3rd shock	SRC0	15/09/1976	A	5.9	16.9
ITACA	IT0103	Friuli earthquake 4th shock	SRC0	15/09/1976	A	5.9	16.4
ITACA	IT0275	Val comino earthquake	ATN	11/05/1984	A	5.5	19.2
ITACA	IT0642	Molise 1st shock	GLD	31/10/2002	A	5.7	25.6
ITACA	IT0650	Molise 2nd shock	GLD	01/11/2002	A	5.7	26.7
ITACA	IT0788	L'Aquila Mainshock	ANT	06/04/2009	A	6.3	23.0
ITACA	IT0806	L'Aquila Mainshock	FMG	06/04/2009	A	6.3	19.3
ITACA	IT0809	L'Aquila Mainshock	GSG	06/04/2009	A	6.3	22.6
ITACA	IT0813	L'Aquila Mainshock	MTR	06/04/2009	A	6.3	22.3
ITACA	IT0870	L'Aquila Earthquake	AQG	07/04/2009	A	5.6	15.1
ITACA	IT0877	L'Aquila Earthquake	CLN	07/04/2009	A	5.6	21.6
ITACA	IT0882	L'Aquila Earthquake	FMG	07/04/2009	A	5.6	28.6
ITACA	IT0883	L'Aquila Earthquake	GSG	07/04/2009	A	5.6	21.7

Table 3 Scale factors for the spectrum-compatible combination of records Comb. 2

Structure 1		Structure 2		Structure 3		Structure 4	
ID	Scale Factors	ID	Scale Factors	ID	Scale Factors	ID	Scale Factors
000128	4.68	000234	2.70	000128	5.77	000128	6.65
000212	2.97	000246	3.50	000234	4.85	000359	6.33
000234	3.03	000368	5.52	000246	5.47	000363	2.83
000246	3.01	000385	7.26	000368	4.79	000368	4.44
000368	3.61	000410	6.45	000410	2.85	000410	3.09
000385	6.54	000642	3.17	000642	4.28	000642	4.28
000410	5.65	000665	1.64	000949	2.63	000949	3.16
000642	3.74	000764	5.47	001243	3.10	001243	3.23
000665	1.07	000949	2.95	006327	4.50	005272	8.01
000949	4.59	001243	1.51	006331	3.98	006115	2.07
001243	1.69	005272	8.98	006333	8.03	006331	4.32

Table 3 Continued

Structure 1		Structure 2		Structure 3		Structure 4	
ID	Scale Factors	ID	Scale Factors	ID	Scale Factors	ID	Scale Factors
006115	1.74	006277	0.76	006335	1.74	006333	7.17
006277	0.59	006327	5.22	006336	3.31	006336	2.92
006331	5.17	006331	7.07	006341	2.10	006341	2.09
006333	8.27	006335	1.68	IT0083	7.43	IT0083	9.16
006335	1.40	006341	4.53	IT0103	1.27	IT0103	1.14
006341	4.60	006342	4.06	IT0788	8.52	IT0642	11.7
006342	3.73	IT0103	1.20	IT0809	8.43	IT0788	9.70
IT0090	3.32	IT0788	6.57	IT0813	4.44	IT0806	8.54
IT0103	1.72	IT0813	5.17	IT0870	3.47	IT0813	3.35

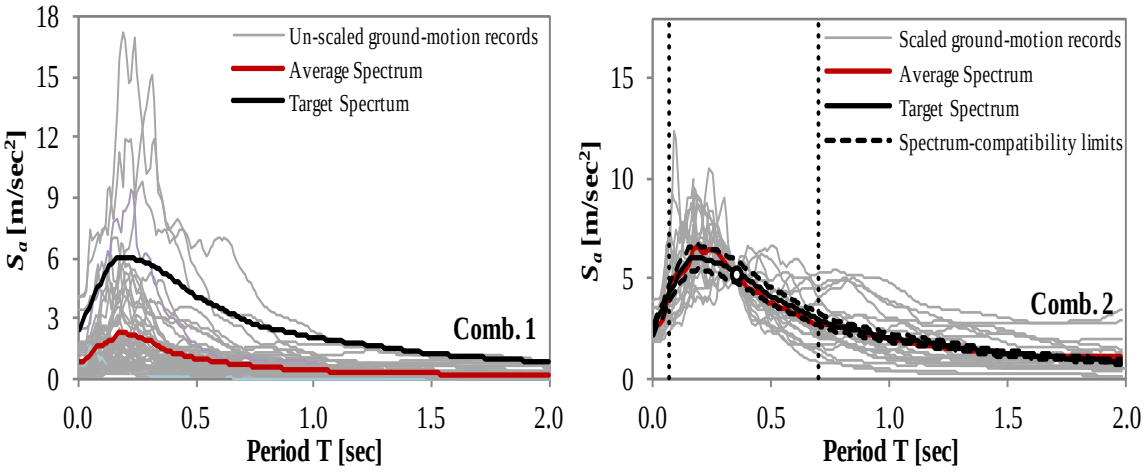

Fig. 2 Combination of records selected for Structure 1

Table 2 identifies all 61 un-scaled ground motion records selected for Comb. 1, while Table 3 specifies the scale factors used for the 20 records belonging to Comb. 2. As an example, Fig. 2 compares the spectra corresponding to the combinations of records selected for Structure 1 and the uniform hazard spectrum obtained from the PSHA (target spectrum).

4. Results and discussion

4.1 NLTHAs with un-scaled ground motion records

The MIDRs obtained by NLTHAs of the four structures of Fig. 1 using all 61 pairs of un-scaled accelerograms of Comb. 1 are summarized in the polar graphs shown in Fig. 3. For Structure 1, which has the most regular configuration, the scatter in the MIDR is similar for all incidence angles, while for the other structures the MIDR varies significantly, depending on the incidence angle. For example, for Structure 3, the maximum MIDR over all incidence angles θ, MIDR(θ), is found for an incidence angle θ = 22.5° and is equal to MIDR(22.5°) = 2.37%.

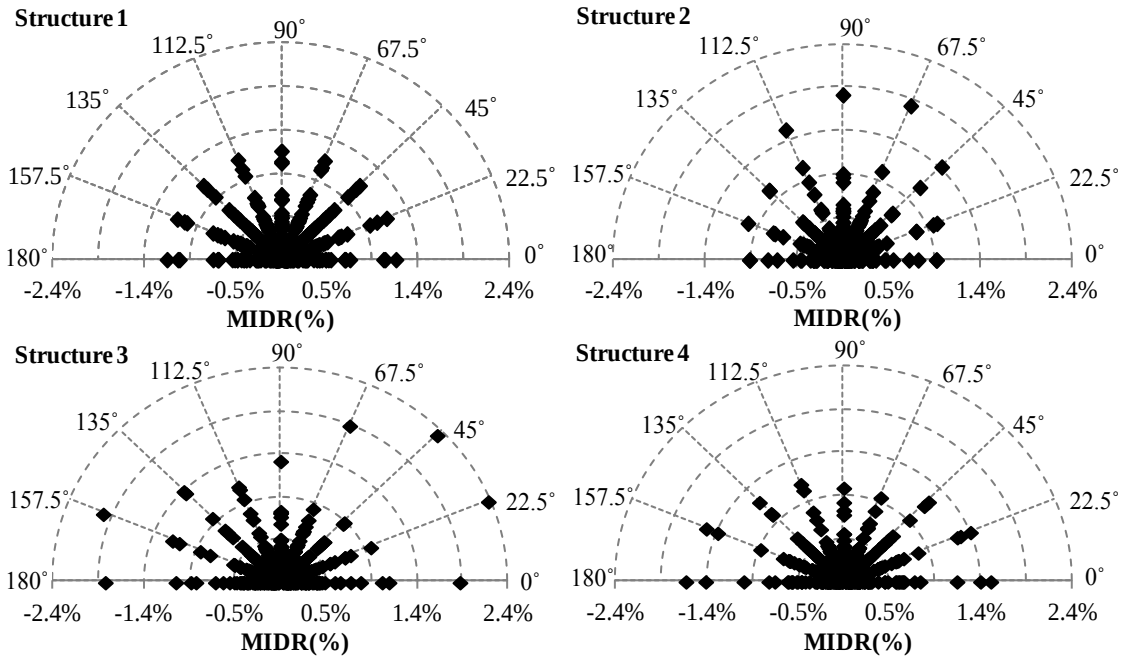

Fig. 3 MIDR of Structures 1, 2, 3 and 4 as a function of the incidence angle for the 61 pairs of un-scaled accelerograms (Comb. 1)

The results of Fig. 3 may be better interpreted if they are normalized with respect to the deformation demand obtained by applying the seismic input with an incidence angle $\theta = 0°$. Athanatopoulou (2005) propose to use the orientation effect ratio, $r(\theta_i)$, to evaluate the directionality effects of the seismic demand. As shown in Eq. (5), the application of the orientation effect ratio $r(\theta_i)$ to the selected EDP relates the MIDR obtained for an incident angle $\theta = \theta_i$ to the MIDR corresponding to an input record aligned with the structural reference axes (i.e. $\theta = 0$).

$$r(\theta_i) = \frac{\mathrm{MIDR}(\theta_i, t)}{\mathrm{MIDR}(t)} \tag{5}$$

where

• θ is the orientation of the two horizontal excitation axes with respect to the structure reference axes; the translational components of ground motions are oriented according to the angles θ and $\theta + 90$ degrees;

• $\mathrm{MIDR}(\theta_i, t)$ is the MIDR for an incident angle $\theta = \theta_i$

• $\mathrm{MIDR}_{0°}(t)$ is the MIDR when the horizontal components of the record are aligned with the structural reference axes (i.e. $\theta = 0$).

Fig. 4 shows the orientation effect ratio $r(\theta_i)$ for the data already shown in Fig. 3. Directionality effects obtained for Structure 2 are much larger than those obtained for the other structures. For this particular structure the maximum $r(\theta_i)$ is 9.14 and it is obtained with record 006331 (database ESD, M_w = 6.4; R = 22 km) applied at an incidence angle $\theta = 67.5°$. The average $r(\theta_i)$ corresponding to the same incidence angle is equal to 1.95.

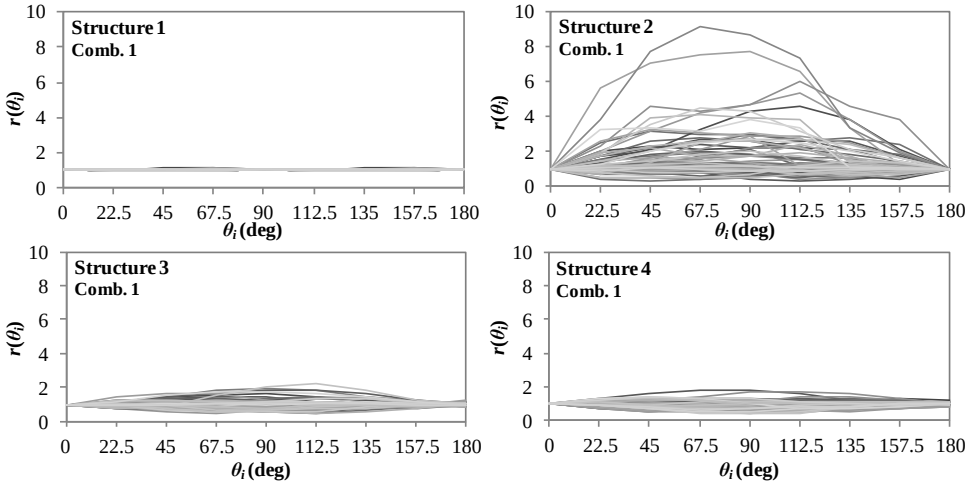

Fig. 4 Variation of MIDR(θ_i) obtained by applying the 61 un-scaled records to Structures 1, 2, 3 and 4

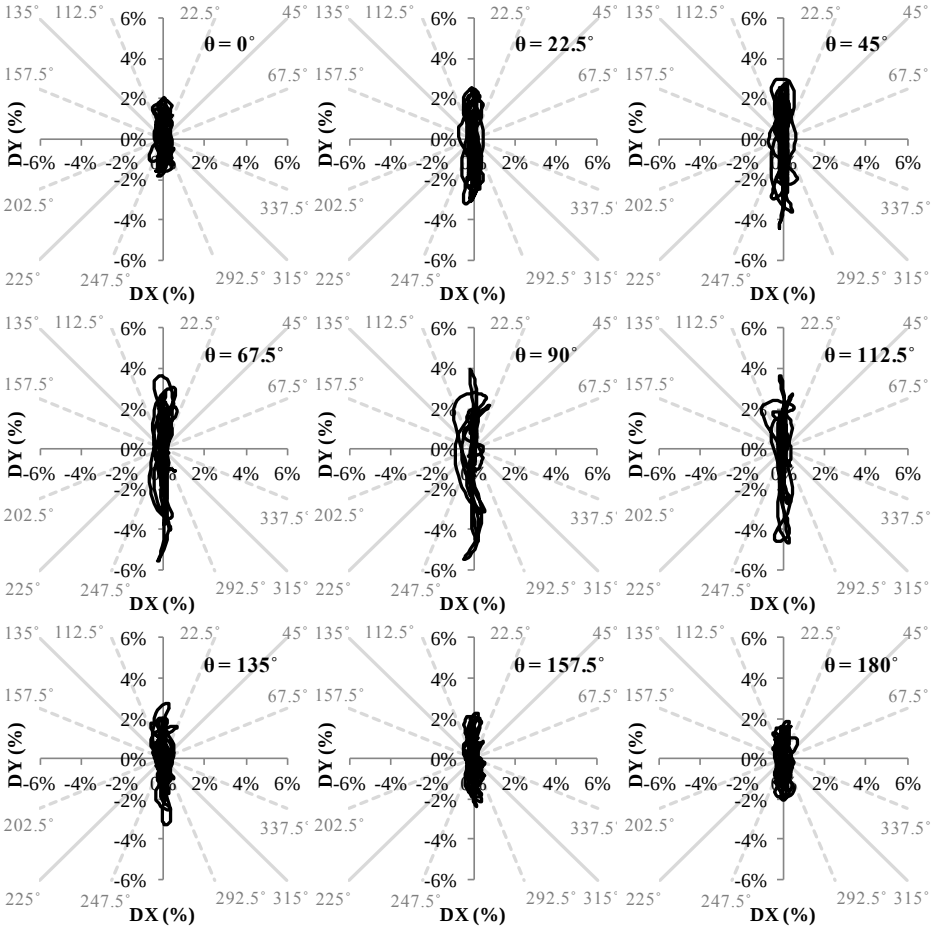

Fig. 5 Interaction between the inter-story drifts DX(t) and DY(t) for Structure 2 subjected to ground motion 000055 (database ESD, M_w = 6.3; R = 23 km) with nine different incidence angles

The incidence angle influence on the seismic demand varies depending on both structural configuration and specific characteristics of each examined record. The influence of the structural configuration is investigated in more detail by analyzing the variation of structural demand on Structure 2 for a single record (000055 from database ESD, M_w = 6.3; R = 23 km) over time. Fig. 5 shows the evolution of DX(t) and DY(t) for the given ground motion. The nine different plots refer to nine different incidence angles. The lack of intermediate bays reduces the capacity of Structure 2 in the Y direction generating a significant difference between the stiffness and strength in its two principal directions. The uncorrelation process (Penzien and Watabe 1975) leads to a first principal component characterized by a larger acceleration intensity than the second principal component. This explains why the DYs are the largest when θ = 90°. This happens when the ground motion first principal component is aligned with the lowest structural capacity direction.

To explain the influence of the characteristics of each record on the seismic demand variation with respect to the incidence angle, the energy content of the 61 selected records is analyzed. The energy content of a single ground motion horizontal *i*-component (with i = X, Y) is evaluated through the Specific Energy Density SED, defined as

$$\mathrm{SED}_i = \int_0^t \left[v_i(t) \right]^2 dt \tag{6}$$

where $v(t)$ is the ground motion velocity and t is the ground motion duration. The SED for the single recorded ground motion is computed as the geometric mean of the SEDs of the two principal components

$$\mathrm{SED} = \sqrt{\mathrm{SED_X} \cdot \mathrm{SED_Y}} \tag{7}$$

Fig. 6 shows the correlations between the SED values corresponding to each un-scaled record and MIDR(θ) of Structure 4 obtained subjected to different incident angles. The measure of the correlation between the two parameters is estimated through the determination coefficients R^2 (Eq. (8)). These coefficients, whose values range between 0 and 1, reveal how closely the predicted value (Y_{pi}) corresponds to the actual data (Y_i)

$$R^2 = \frac{\sum_i^n \left(Y_{pi} - Y_m \right)^2}{\sum_i^n \left(Y_i - Y_m \right)^2} \tag{8}$$

where Y_m = mean value and n = total number of points.

The R^2 coefficients are based on linear and polynomial regression lines fitted through the data. The forms of the linear and polynomial relationships are $y = ax+c$ and $y = ax+bx^2$ respectively, where a, b and c are constant coefficients. Table 4 shows the R^2 values obtained correlating the SED and MIDR values for all analyzed structures and incidence angles. The energy content of the un-scaled records have a good correlation with the seismic demand for Structure 3 and Structure 4. Since these structures have a high non-linear behavior, the effects of inelasticity and ground motion duration are implicitly captured by the energy-based ground motion parameters (Mollaioli *et al*. 2004, Mollaioli *et al*. 2011), as they are directly related to the number of cycles of the oscillator response.

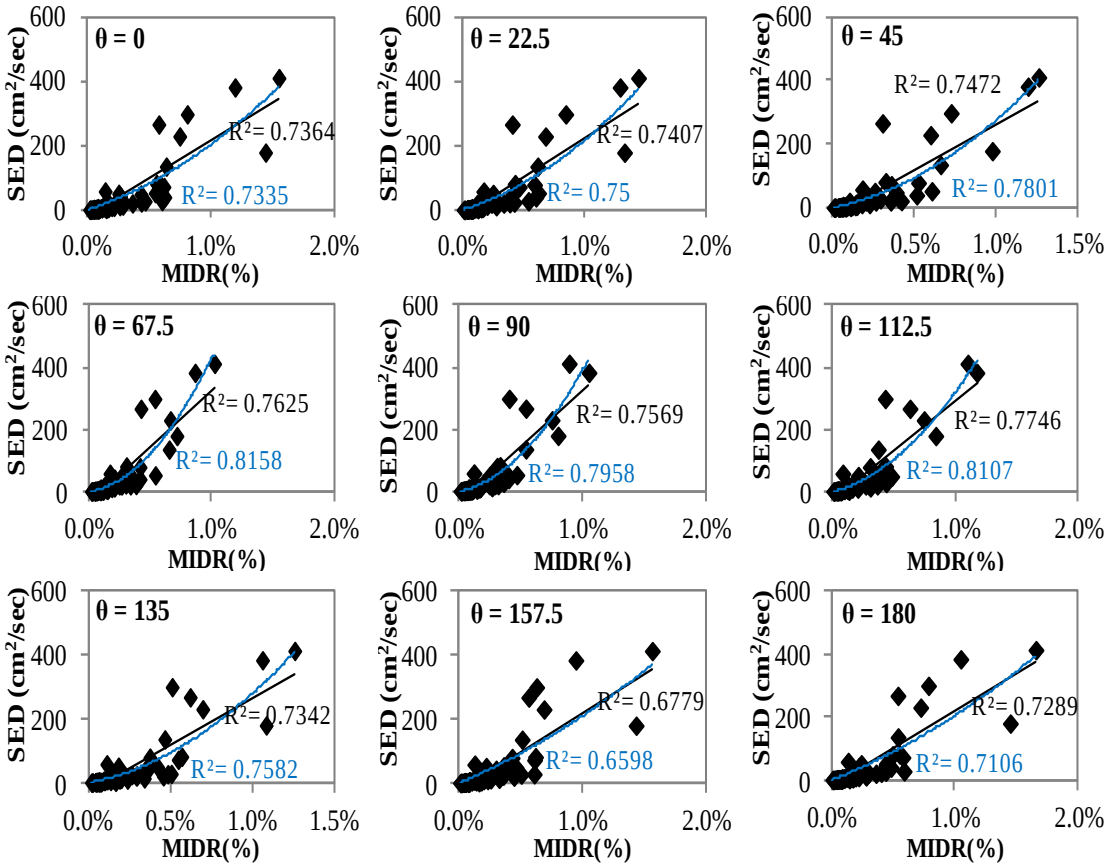

Fig. 6 Correlations between the MIDRs obtained subjecting Structure 4 to 61 ground motion records oriented along nine different incident angles and the corresponding SED values of the seismic inputs

Table 4 Coefficients of determination R^2 from correlations between SED values and MIDRs calculated for all four structures subjected to the 61 un-scaled records selected at the ULS

Coefficients of Determination R^2									
Linear Regression Line					Polynomial Regression Line				
θ_i	Str. 1	Str. 2	Str.3	Str. 4	θ_i	Str. 1	Str. 2	Str.3	Str. 4
0°	0.4555	0.3979	0.6893	0.7364	**0°**	0.5140	0.4027	0.6783	0.7335
22.5°	0.4401	0.4407	0.6738	0.7407	**22.5°**	0.4902	0.4630	0.6567	0.7500
45°	0.4310	0.4788	0.6753	0.7472	**45°**	0.4871	0.4948	0.6588	0.7801
67.5°	0.4421	0.5301	0.7508	0.7625	**67.5°**	0.5047	0.5372	0.7090	0.8158
90°	0.4555	0.5444	0.7891	0.7569	**90°**	0.5140	0.5588	0.7861	0.7958
112.5°	0.4401	0.5940	0.7310	0.7746	**112.5°**	0.4902	0.6304	0.7684	0.8107
135°	0.4310	0.5423	0.7154	0.7342	**135°**	0.4871	0.6039	0.7082	0.7582
157.5°	0.4421	0.4865	0.7129	0.6779	**157.5°**	0.5047	0.5218	0.6986	0.6598
180°	0.4555	0.3979	0.7067	0.7289	**180°**	0.5140	0.4027	0.6895	0.7106

4.2 NLTHAs with scaled and spectrum-compatible ground motion records

Fig. 7 shows the variation of the orientation effect ratios $r(\theta_i)$ obtained subjecting the four analyzed structures to the combination of scaled records with nine different incidence angles. As expected, the directionality effects are larger for the irregular structures (Structures 2, 3, 4). For example, Comb. 2 applied to Structure 3 along $\theta = 112.5°$ produces a maximum orientation effect ratio $r(\theta_i)_{max}$ equal to 4.83 and an average $r(\theta_i)$ equal to 1.22.

The comparison of Fig. 4 and Fig. 7 shows that directionality effects are more relevant when un-scaled records are used. This behavior partially depends on the limitation of the uncertainty in the records imposed by a record selection based on the spectrum-compatibility criterion applied in this study.

Similarly to the results obtained for the un-scaled records, for the spectrum-compatible scaled records the influence of the incidence angle on the seismic demand varies depending on both the structural irregularity and the specific characteristics of the single record. The influence of the structural configuration on the directionality effects is analyzed comparing the structural capacities corresponding to the main principal axes and the direction that yields the maximum $r(\theta_i)$. Structural capacities are evaluated through pushover curves corresponding to mass proportional lateral forces oriented along the directions θ_i. For Structure 3, the pushover capacity curves for $\theta_i = 0°$, 90° and 112.5° are shown in Fig. 8 and reveal that the strength for $\theta = 0°$ is considerably higher than for $\theta = 90°$ and $\theta = 112.5°$. This explains why for Structure 3 in Fig. 7 the maximum $r(\theta_i)$ is obtained at $\theta = 112.5°$, the direction with the lowest capacity.

Some records, for specific incidence angles, generate EDPs much larger than others having similar or lower spectral accelerations, in the same spectrum-compatibility range. For example, record 006333 (database ESD, $M_w = 6.4$; R = 28 km) at $\theta = 112.5°$ produces on Structure 3 much

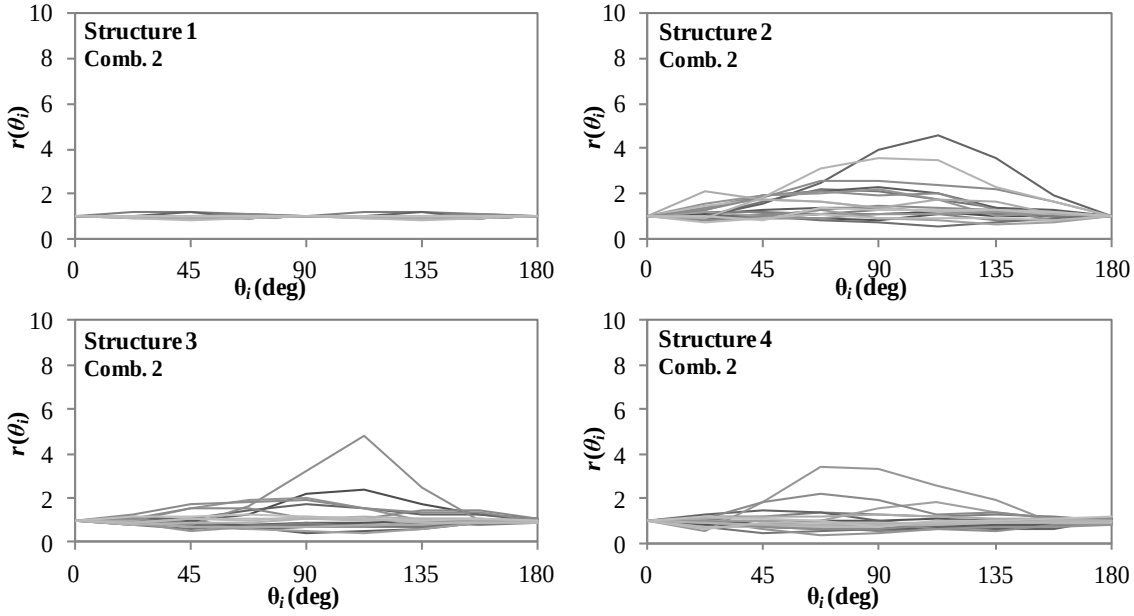

Fig. 7 $r(\theta_i)$ variation for Structures 1, 2, 3 and 4 for the combination of spectrum-compatible records

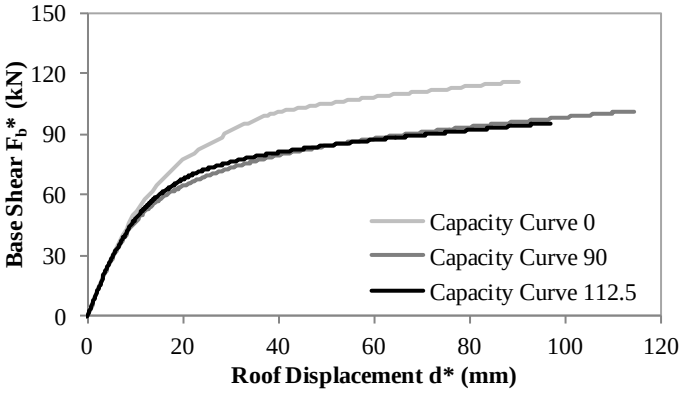

Fig. 8 Pushover curves of Structure 3 for mass proportional lateral forces oriented along θ_i = 0°, 90° and 112.5°

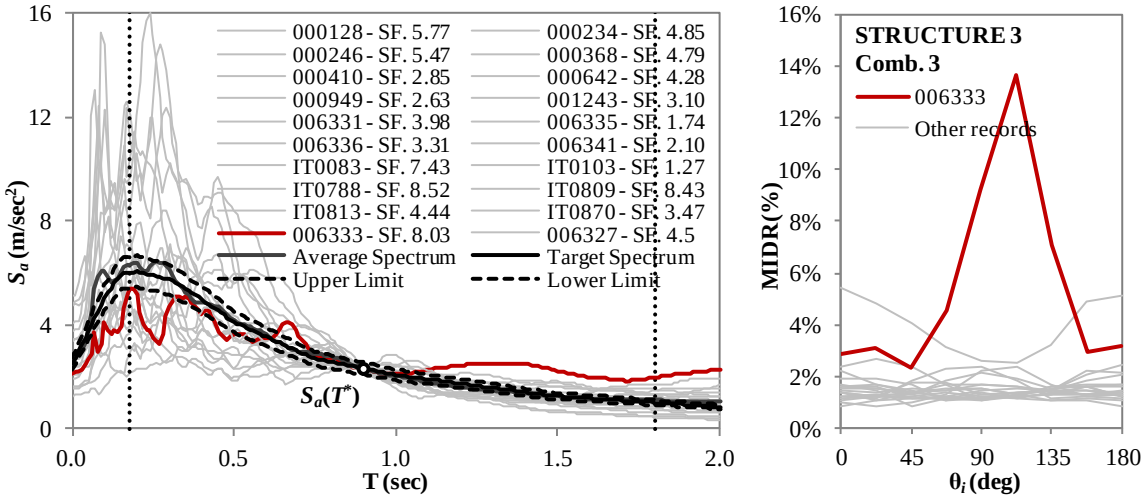

Fig. 9 Scaled response spectra for records belonging to the spectrum-compatible scaled combination Comb. 2 (on the left) and variation of the MIDR(θ_i) produced subjecting Structure 3 to the records of Comb. 2 (on the right)

higher MIDRs than other records belonging to the same spectrum-compatible combination (Comb.2), even if the response spectrum acceleration values obtained with record 006333 are apparently smaller than those of the other records (Fig. 9).

In order to understand this behavior, the energy contents of the records belonging to Comb.2 are analyzed and compared. The records' energy is evaluated by an Energy Flux EF plot, representing the SED increasing over time. Similarly to SED in Eq. (7), EF(t) is computed as the geometric mean of the two components

$$\mathrm{EF}(t) = \sqrt{\mathrm{EF_X}(t) \cdot \mathrm{EF_Y}(t)} \tag{9}$$

EF(t) captures the cumulative kinetic energy input on the structure during the earthquake. Fig. 10

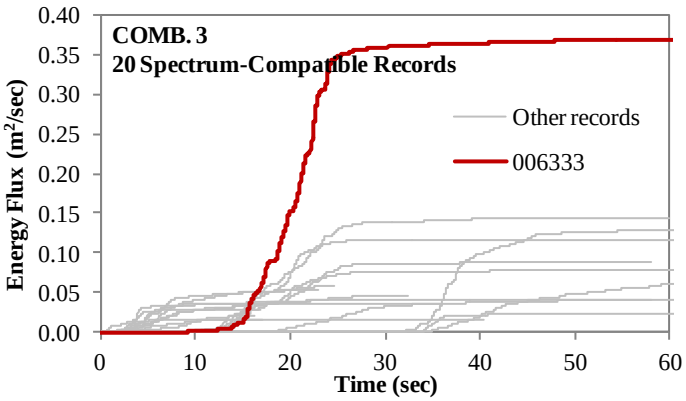

Fig. 10 Energy Flux plots of the records belonging to the spectrum-compatible Combination 3

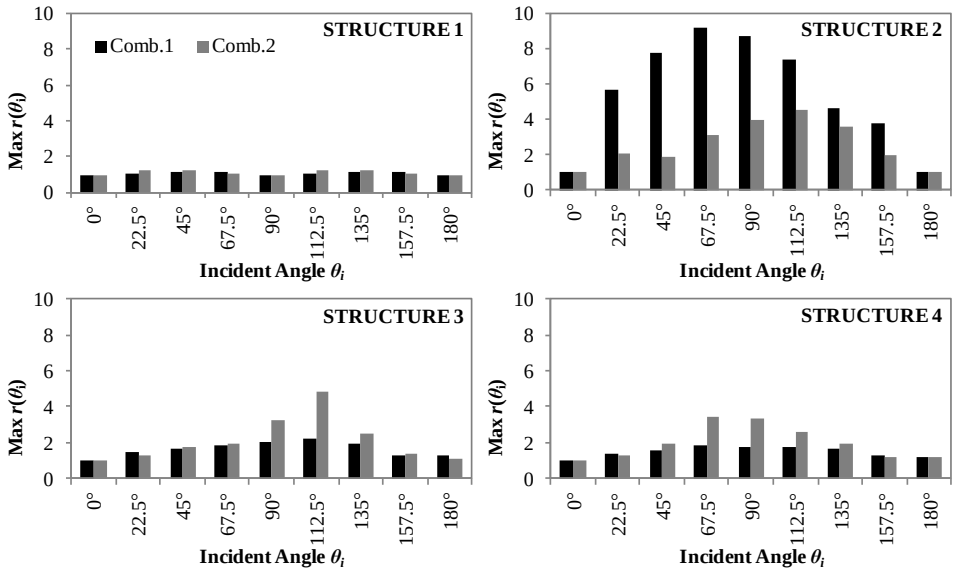

Fig. 11 Maximum $r(\theta_i)$ for Structures 1, 2, 3 and 4 for the two record combinations

shows the EF(t) plots for all ground motion records belonging to Comb.2. The EF(t) plots confirm that the recordings with higher energy content produce higher MIDRs, even more so along the direction in which the structure is characterized by the lowest capacity, as indicated by the large plastic MIDR(θ) in Fig. 9.

4.3 Comparison between results obtained with un-scaled and scaled ground motion records

Fig. 11 compares the maximum orientation effects $r(\theta_i)_{max}$ generated for each analyzed record combination of records and for each structure. $r(\theta_i)_{max}$ obtained from the scaled and spectrum-compatible combinations is lower than that computed for the un-scaled accelerograms; $r(\theta_i)_{max}$ =

9.14 is obtained by subjecting Structure 2 to the un-scaled records of Comb.1.

Fig. 11 also indicates that the records of Comb.2 yield high $r(\theta_i)_{max}$ on Structure 3 and Structure 4. As shown in the previous paragraph, this results depends on the scaled record 006333 of Comb.2, which produces MIDR much higher than other records (Fig. 9). However, the same un-scaled record does not produce such large MIDR. This can be explained comparing the energy content of the scaled and un-scaled record through the analysis of the corresponding SED values. When record 006333 is un-scaled, it is characterized by a SED equal to 0.0057 m^2/sec, while when the same record is scaled - for example to the $S_a(T^*)$ of Structure 3 - SED is equal to 0.37 m^2/sec. The high scaling factors used for several records (for record 006333, SF = 8.03) significantly modify the record energy content. High scaling factors produce large MIDR in particular when the principal component of the un-correlated record is oriented along the minimum structural capacity direction. When a structure is characterized by a high structural period (as for Structure 3 with T^* = 0.9 sec), the spectrum-compatibility range required by Eurocode 8 (UNI EN 1998-1:2005), that is 0.2T to 2T, becomes very large, thus forcing the use of records having large scale factors. In this case, it is very difficult or even impossible to select ground motions having low scaling factors which are spectrum-compatible because of the scarcity of records with these characteristics within current ground motion databases. This issue must be considered in the selection of the scaling and compatibility criteria. Although strict limits on scaling are not imposed, many authors recommend using scaling factors as close to unity as possible (Bommer *et al*. 2004). Krinitzsky and Chang (1977) and Vanmarke (1979) propose that if scaling factors larger than 4 need to be applied to accelerograms, the records should be rejected. As shown in this section, the rationale behind imposing limits on scaling is to avoid creating unrealistic ground motion records, as is the case, in this paper, of record 006333. In order to avoid improbable structural responses, it would be advisable to set an upper limit to the scaling factor.

5. Conclusions

This paper investigates the critical responses of four regular and irregular structures subjected to several ground motion records applied along different incidence angles, ranging between 0 and 180 degrees, with 22.5 degree increments. The structural response is assessed through Non-Linear Time History Analyses. Since this work also investigates the influence of the ground motion selection and scaling method on directionality effects, the considered ground motion inputs consist of both scaled and un-scaled records with two horizontal un-correlated components. The un-scaled records consist of 61 pairs of accelerograms selected for a 10% in 50 years probability of exceedance scenario, while the scaled ground motions consist of a combination of spectrum-compatible records, with 20 pairs of accelerograms, scaled to the non-linear spectral acceleration $S_a(T^*)$. The principal results presented in this paper can be summarized as follows

1. The structural demand on a doubly-symmetric, regular, 1-storey reinforced concrete structure does not vary significantly with the incidence angle. Conversely, MIDRs for plan-irregular reinforced concrete structures vary considerably depending on the incidence angle.
2. The analysis of the maximum orientation effect ratios $r(\theta_i)_{max}$ obtained from the un-scaled ground motions shows significant differences between the EDP computed by applying the seismic input along different incidence angles. This behavior depends on the plan-irregularity of the buildings, which produces significantly different stiffness and capacity

in different directions. The applied ground motion generates the highest demand when applied to the direction with the minimum structural capacity.

3. Correlations between the energy content, measured by the Specific Energy Density SED, of the 61 un-scaled records and the MIDRs obtained applying the ground motions at different incidence angles, show that the demand on the plan-irregular structures is well correlated with the ground motion SEDs. High energy content records tend to produce high MIDR(θ), when they are applied to the structural direction with the lowest capacity. For regular structures this trend is not as visible because their behavior, in terms of flexibility and strength, does not vary significantly along different directions.
4. The NLTHAs carried out with the set of spectrum-compatible scaled accelerograms confirm that ground motion records applied to irregular structures with different incident angles produce EDPs which are affected by the earthquake direction. Higher values of MIDR(θ) and $r(\theta_i)$ are obtained when the ground motions are applied to the irregular structures.
5. The influence of the structural configuration on the directionality effects generated from spectrum-compatible scaled records is analyzed comparing the structural capacities along the main structural axes and the direction generating $r(\theta_i)_{max}$. The pushover curves show that the structural capacity significantly varies as a function of the loading direction. More specifically, the lowest strength direction corresponds to the direction producing the maximum EDP and $r(\theta_i)$.
6. The comparison of the results obtained from scaled and un-scaled records point out that the directionality effects are in general lower than those obtained for the un-scaled records when scaled spectrum-compatible records are used. The ground motions generating the maximum demands are those with the highest energy content, measured by the SED. In order to control the uncertainty of the seismic demand, the authors suggests to control the energy content of the records used in NLTHA by a selection of ground motion records that limits the variability of the SED values (or other energy parameters).
7. The use of high scaling factors significantly modifies the SED, generating unrealistically high structural demands in the directions with the lowest capacity. In order to avoid the above danger, it is therefore recommended to use upper limits for the scaling factor, as proposed in the published literature. Bommer and Acevedo (2004) suggest to use a scaling factor as close as possible to one, while Krinitzsky and Chang (1977) and Vanmarke (1979) limit the scaling factor to 4.

The results of this study apply more specifically to existing buildings, which often present irregularities in plan and height, with stiffness and strength that may vary significantly according to the loading direction. Older buildings, designed for gravity loads only, tend to show weak column-strong beam behaviors, as modeled in the four structures presented in this study. In these cases, the NLTHAs performed by applying the ground motion records along the principal axes can substantially underestimate the structural demand prediction. In order to avoid unrealistic responses it is very important to control the energy contents of the ground motions used for NLTHA and to limit the scale factors used to obtain the spectrum compatible records.

References

Ambraseys, N., Smit, P., Sigbjornsson, R., Suhadolc, P. and Margaris, B. (2002), *Internet-Site for European*

Strong-Motion Data, European Commission, Research-Directorate General, Environment and Climate Programme.

Athanatopoulou, A.M. (2005), "Critical orientation of three correlated seismic components", *Eng. Struct.*, **27**(2), 301-312.

Baker, J.W. (2011), "Conditional mean spectrum: Tool for ground-motion selection", *J. Struct. Eng.*, **137**(3), 322-331.

Baker, J.W. and Cornell, A.C. (2005), "A vector-valued ground motion intensity measure consisting of spectral acceleration and epsilon", *Earthq. Eng. Struct. Dyn.*, **34**(10), 1193-1217.

Bazzurro, P. and Cornell, C.A. (1999), "Disaggregation of seismic hazard", *Bull. Seismol. Soc. Am.*, **89**(2), 501-520.

Beyer, K. and Bommer, J.J. (2006), "Relationships between median values and between aleatory variabilities for different definitions of the horizontal component of motion", *Bull. Seismol. Soc. Am.*, **96**(4A), 1512-1522.

Bommer, J.J. and Acevedo, A.B. (2004), "The use of real earthquake accelerograms as input to dynamic analysis", *J. Earthq. Eng.*, **8**(Special Issue 1), 43-91.

Cantagallo, C., Camata, G., Spacone, E. and Corotis, R. (2012), "The variability of deformation demand with ground motion intensity", *Probab. Eng. Mech.*, **28**, 59-65.

CEN – EN 1998-1 (2004), *Design of structures for earthquake resistance - Part 1: General rules, seismic actions and rules for buildings*, Eurocode 8.

Faggella, M., Barbosa, A.R., Conte, J.P., Spacone, E. and Restrepo, J.I. (2013), "Probabilistic seismic response analysis of a 3-D reinforced concrete building", *Struct. Safety*, **44**, 11-27.

Hosseini, M. and Salemi, A. (2008), "Studying the effect of earthquake excitation on the internal forces of steel building's elements by using nonlinear time history analyses", *Proceedings of the 14th World Conference on Earthq. Eng.*, Bejing, China, October.

Iervolino, I., Maddaloni, G. and Cosenza, E. (2008), "Eurocode 8 compliant record sets for seismic analysis of structures", *J. Earthq. Eng.*, **12**, 54-90.

Kalkan, E. and Reyes, J.C. (2013), "Significance of rotating ground motions on behavior of symmetric- and asymmetric-plan structures: Part 2. multi-story structures", *Earthq. Spectra*, doi: http://dx.doi.org/10.1193/072012EQS242M.

Kent, D.C. and Park, R. (1971), "Flexural members with confined concrete", *J. Struct. Div. ASCE*, **97**(7), 1969–1990.

Krinitzsky, E.L. and Chang, F.K. (1977), *State-of-the-art for Assessing Earthquake Hazards in the United States: Specifying Peak Motions for Design Earthquakes*, Miscellaneous Paper S-73-1, Report 7, U.S. Army Engineers Waterways Experiment Station, Vicksburg, Mississippi.

Lagaros, N. (2010), "Multicomponent incremental dynamic analysis considering variable incident angle", *Struct. Infrastruct. Eng.*, **6**(2), 77-94.

Lopez, O.A., Chopra, A.K. and Hernandez, J.J. (2000), "Critical response of structures to multi-component earthquake excitations", *Earthq. Eng. Struct. Dyn.*, **29**(12), 1759-1778.

Lopez, A. and Hernández, J.J. (2004), "Structural design for multicomponent seismic motion", *Proceedings of the 13th World Conference on Earthquake Engineering*, Vancouver, B.C., Canada, August.

Lopez, O.A., and Torres, R. (1997), "The Critical angle of seismic incidence and the maximum structural response", *Earthq. Eng. Struc. Dyn.*, **26**(9), 881-894.

Luzi, L., Hailemikael, S., Bindi, D., Pacor, F., Mele, F. and Sabetta, F. (2008), ITACA (ITalian ACcelerometric Archive): A Web Portal for the Dissemination of Italian Strong-motion Data, *Seismol. Res. Lett.*, **79**(5), 716–722.

Meletti, C. and Montaldo, V. (2007), *Stime di Pericolosità Sismica per Diverse Probabilità di Superamento in 50 Anni: Valori di* a_g, Progetto DPC-INGV S1, Deliverable D2 2007; http://esse1.mi.ingv.it/d2.html.

Menegotto, M. and Pinto, P.E. (1973), "Method of analysis for cyclically loaded r. c. plane frames including changes in geometry and non-elastic behavior of elements under combined normal force and bending", IABSE Symposium: *Resistance and Ultimate Deformability of Structures Acted on by Well Defined*

Repeated Loads - IABSE, Lisboa, Portugal.
Menum, C. and Der Kireghian, A. (1998), "A replacement for the 30%, 40%, and SRSS rules for multicomponent seismic analysis", *Earthq. Spectra*, **14**(1), 153-164.
Mollaioli, F., Bruno, S., Decanini, L. and Saragoni, R. (2004), "On the correlation between energy and displacement", *Proceedings of the 13th World Conference on Earthquake Engineering*, Vancouver, B.C., Canada, August.
Mollaioli, F., Bruno, S., Decanini, L. and Saragoni, R. (2011), "Correlations between energy and displacement demands for performance-based seismic engineering", *Pure Appl. Geophysics*, **168**(1-2), January 2011, 237-259.
Pacor, F., Paolucci, R., Luzi, L., Sabetta, F., Spinelli, A., Gorini, A., Nicoletti, M., Marcucci, S., Filippi, L. and Dolce, M. (2011), "Overview of the Italian strong motion database ITACA 1.0", *Bull. Earthq. Eng.*, **9**(6), 1723–1739.
Penzien, J. and Watabe, M. (1975), "Characteristics of 3-dimensional earthquake ground motion. Earthquake", *Eng. Struct. Dyn.*, **3**(4), 365-374.
Reyes, J.C. and Kalkan E. (2012), "Relevance of Fault-Normal/Parallel and maximum direction rotated ground motions on nonlinear behavior of multi-story buildings", *Proceedings of the 15th World Conference on Earthquake Engineering*, Lisboa, Portugal.
Rigato, A.B. and Medina R.A. (2007), "Influence of angle of incidence on seismic demands for inelastic single-storey structures subjected to bi-directional ground motions", *Eng. Struct.*, **29**(10), 2593-2601.
Smeby, W. and Der Kiureghian, A. (1985), "Modal combination rules for multicomponent earthquake excitation", *Earthq. Eng. Struct. Dyn.*, **13**(1), 1-12.
Spacone, E., Filippou, F.C. and Taucer, F. (1996), "Fiber beam-column model for nonlinear analysis of R/C frames: I. formulation", *Earthq. Eng. Struct. Dyn.*, **25**(7), 711-725.
Spallarossa, D. and Barani, S. (2007), *Disaggregazione Della Pericolosità Sismica in Termini di M-R-ε*, Progetto DPC-INGV S1, Deliverable D14 2007, http://esse1.mi.ingv.it/d14.html.
Stewart, J.P., Abrahamson, N.A., Atkinson, G.M., Baker, J., Boore, D.M., Bozorgnia, Y., Campbell, K.W., Comartin, C.D., Idriss, I.M., Lew, M., Mehrain, M., Moehle, J.P., Naeim, F. and Sabol, T.A. (2011), "*Representation of Bi-directional Ground Motions for Design Spectra in Building Codes*", *Earthq. Spectra*, **27**(3), 927-937.
Tsourekas, A., Athanatopoulou, A. and Avramidis I. (2009), "Effects of seismic incident angle on response of structures under bi-directional recorded and artificial ground motion", *ECCOMAS Thematic Conference on Computational Methods in Structural Dynamics and Earthquake Engineering (COMPDYN)*, Rhodes, Greece.
Vanmarke, E.H. (1979), *Representation of Earthquake Ground Motion: Scaled Accelerograms and Equivalent Response Spectra. State-of-the-Art for Assessing Earthquake Hazards in the United States*, Miscellaneous Paper S-73-1, Report 14, U.S. Army Engineers Waterways Experiment Station, Vicksburg, Mississippi.
Wilson, E., Suharwardy, I. and Habidullah, A. (1995), "A clarification of the orthogonal effects in a three-dimensional seismic analysis", *Earthq. Spectra*, **11**(4), 659-666.